

Chiral electric field in relativistic heavy-ion collisions at energies available at the BNL Relativistic Heavy Ion Collider and at the CERN Large Hadron Collider

ZHONG Yang(钟洋)^{1,2,*)} YANG Chun-Bin (杨纯斌)^{1,3}, CAI Xu (蔡勖)^{1,3}

FENG Sheng-Qin(冯笙琴)^{2,3}

¹Institute of Particle Physics, Central China Normal University, Wuhan 430079, China

²Department of Physics, College of Science, China Three Gorges University,
Yichang 443002, China

³Key Laboratory of Quark and Lepton Physics (Huazhong Normal University),
Ministry of Education, Wuhan 430079, China

Abstract: It was proposed that the electric fields may lead to chiral separation in QGP, which is called the chiral electric separation effect. The strong electromagnetic field and the QCD vacuum can both completely be produced in the off-central nuclear-nuclear collision. We used the Wood-Saxon nucleon distribution to calculate the electric field distributions of the off-central collisions. The chiral electro field spatial distribution at Relativistic Heavy-Ion Collider (RHIC) and Large Hadron Collider (LHC) energy regions are systematically studied in this paper. Compared with magnetic field spatial distribution, electric field shows some different features in relativistic heavy-ion collisions. The dependence of the electric field produced by the thermal quark in the central position with different impact parameters on the proper time with different collision energies in the RHIC and LHC energy region are studied in this paper.

Keywords: Spatial distribution of electric field, chiral electric field

PACS: 25.75.Ld, 11.30.Er, 11.30.Rd

1 Introduction

Relativistic heavy-ion collisions generate not only hot quark-gluon plasma (QGP) but also large magnetic fields due to the colliding ions fast motion [1-6]. Relativistic heavy-ion collisions can also generate strong electric fields due to the event-by-event fluctuation of the proton positions in the ions [3,5]. It was proposed that the electric fields may also lead to chiral separation in QGP, which is called the chiral electric separation effect (CESE) [7–11].

* Supported by National Natural Science Foundation of China (Grants Nos. 11375069, 11435054, 11075061, and 11221504), Excellent Youth Foundation of Hubei Scientific Committee (2006ABB036) and Key Laboratory foundation of Quark and Lepton Physics (Hua-Zhong Normal University)(QLPL2014P01)

1) Corresponding author: yzhong913@163.com

The origin of electromagnetic field in relativistic heavy-ion collisions comes from collisions of two ions of radius R with electric charge Ze and extremely high velocity at impact parameter b . Lots of analytical and numerical calculations indicate existence of extremely powerful electromagnetic fields in relativistic heavy-ion collisions [1-5]. It is generally believed that this is the maximum electromagnetic field that nature can produce.

Kharzeev, McLerran and Warringa (KNW) [10] presented a novel mechanism for the study of charge separation of chiral magnetic effect. The topological charge changing transitions provide the parity (P) and CP violations necessary for charge separation. The variance of the net topological charge change is proportional to the total number of topological charge changing transitions. Therefore if sufficiently hot matter is produced in relativistic heavy-ion collisions so that topological charge transitions can take place.

In Refs [12, 13], we used the Wood-Saxon nucleon distribution to replace that of the uniform distribution to improve the magnetic field calculation of the off-central collision based on the theory of KMW [10]. The study of the chiral magnetic field distribution at Relativistic Heavy-Ion Collider (RHIC) and Large Hadron Collider (LHC) energy regions has been carried out in Refs. [10, 12, 13]. In this paper, we will calculate the spatial distribution feature of the electric field in the RHIC and LHC energy regions. The electric field distributions of total charges by the produced thermal quarks are also studied in the paper.

The paper is organized as follows. The study of background electric field in relativistic heavy-ion collisions is present in Sec. II. The electric field distributions of total charges by the produced thermal quarks are present in Sec. III. A summary is provided in Sec. IV.

2 The study of background electric field in relativistic heavy-ion collisions

As the nuclei travel with the speed of light in ultra-relativistic heavy-ion collision experiments, the Lorentz contraction factor γ is so large that the two colliding nuclei can be taken as pancake shape (as the $z = 0$ plane). The Wood-Saxon nuclear distribution is used in Ref. [12, 13] to calculate the magnetic field. The Wood-Saxon nuclear distribution form is as follows:

$$n_A(r) = \frac{n_0}{1 + \exp(\frac{r-R}{d})}, \quad (1)$$

where $n_0 = 0.17 fm^{-3}$, $d = 0.54 fm$ and $R = 1.12 A^{1/3} fm$. The density of the two-dimensional plane can be given as:

$$\rho_{\pm}(\vec{x}'_{\perp}) = N \cdot \int_{-\infty}^{\infty} dz' \frac{n_0}{1 + \exp(\frac{\sqrt{(x' \mp b/2)^2 + y'^2 + z'^2} - R}{d})}, \quad (2)$$

where N is the normalization constant. The number density function $\rho_{\pm}(\vec{x}'_{\perp})$ should be normalized as

$$\int d\vec{x}'_{\perp} \rho_{\pm}(\vec{x}'_{\perp}) = 1. \quad (3)$$

The specific forms of the expression for the electric field in the following way

$$\vec{E} = \vec{E}_p^+ + \vec{E}_p^- + \vec{E}_s^+ + \vec{E}_s^-, \quad (4)$$

where \vec{E}_p^{\pm} and \vec{E}_s^{\pm} are the contributions of the participants and spectators moving in the positive and negative directions, respectively. The contribution of the participants to the electric field is given by

$$\vec{E}_p^{\pm} = \pm Z \alpha_{EM} \int d^2 \vec{x}'_{\perp} \int dY f(Y) \cosh(Y \mp \eta) \rho_{\pm}(\vec{x}'_{\perp}) \theta_{\mp}(\vec{x}'_{\perp}) \frac{\vec{x}'_{\perp} - \vec{x}_{\perp}}{\left[(\vec{x}'_{\perp} - \vec{x}_{\perp})^2 + \tau^2 \sinh^2(Y + \eta) \right]^{3/2}}, \quad (5)$$

where $\theta_{\mp}(\vec{x}'_{\perp}) = \theta\left[R^2 - (\vec{x}'_{\perp} \pm \vec{b}/2)^2\right]$ is a step function, $\eta = \frac{1}{2} \ln[(t+z)/(t-z)]$ is the space-time rapidity and $\tau = (t^2 - z^2)^{1/2}$ is the proper time. The distribution of participants that remain traveling along the beam axis is given by

$$f(Y) = \frac{a}{2 \sinh(aY_0)} e^{aY}, \quad -Y_0 \leq Y \leq Y_0 \quad (6)$$

where $a \approx 1/2$ is given by experimental data. The x and y components of the \vec{E}_p^{\pm} are given by:

$$\vec{E}_{px}^{\pm} = \pm Z \alpha_{EM} \int d^2 \vec{x}'_{\perp} \int dY f(Y) \cosh(Y \mp \eta) \rho_{\pm}(\vec{x}'_{\perp}) \theta_{\mp}(\vec{x}'_{\perp}) \frac{x' - x}{\left[(\vec{x}' - \vec{x})^2 + \tau^2 \sinh^2(Y + \eta) \right]^{3/2}} \quad (7)$$

$$\vec{E}_{py}^{\pm} = \pm Z \alpha_{EM} \int d^2 \vec{x}'_{\perp} \int dY f(Y) \cosh(Y \mp \eta) \rho_{\pm}(\vec{x}'_{\perp}) \theta_{\mp}(\vec{x}'_{\perp}) \frac{y' - y}{\left[(\vec{x}' - \vec{x})^2 + \tau^2 \sinh^2(Y + \eta) \right]^{3/2}} \quad (8)$$

The contribution of the spectators to the electric field is given by

$$\vec{E}_s^\pm = \pm Z\alpha_{EM} \cosh(Y_0 \mp \eta) [d^2 \vec{x}'_\perp \rho_\pm(\vec{x}'_\perp) [1 - \theta_\mp(\vec{x}'_\perp)] \frac{\vec{x}'_\perp - \vec{x}_\perp}{[(\vec{x}'_\perp - \vec{x}_\perp)^2 + \tau^2 \sinh^2(Y + \eta)]^{3/2}} \quad (10)$$

The x and y components of the \vec{E}_s^\pm are given by:

$$\vec{E}_{sx}^\pm = \pm Z\alpha_{EM} \cosh(Y \mp \eta) [d^2 \vec{x}'_\perp \rho_\pm(\vec{x}'_\perp) [1 - \theta_\mp(\vec{x}'_\perp)] \frac{x' - x}{[(\vec{x}' - \vec{x})^2 + \tau^2 \sinh^2(Y + \eta)]^{3/2}} \quad (11)$$

$$\vec{E}_{sy}^\pm = \pm Z\alpha_{EM} \cosh(Y \mp \eta) [d^2 \vec{x}'_\perp \rho_\pm(\vec{x}'_\perp) [1 - \theta_\mp(\vec{x}'_\perp)] \frac{y' - y}{[(\vec{x}' - \vec{x})^2 + \tau^2 \sinh^2(Y + \eta)]^{3/2}} \quad (12)$$

Fig. 1 shows the dependence of electric field spatial distributions of eE_x on different collision energies $\sqrt{s_{NN}} = 62.4$ GeV, 130 GeV and 200 GeV at proper time $\tau = 0.0001$ fm and impact parameter $b = 8$ fm. The collision energies shown in Fig. 1 are in the RHIC energy region. The spatial distributions eE_x show obviously axis symmetry characteristics along $x = 0$ and $y = 0$ axes. There is a valley at the central point ($x = 0, y = 0$) and magnitudes of the x component of electric field (eE_x) are most case below 10MeV^2 during RHIC energy region. It is interesting to find that the eE_x spatial distributions are not smooth which have some distribution peaks on the surface of spatial distributions.

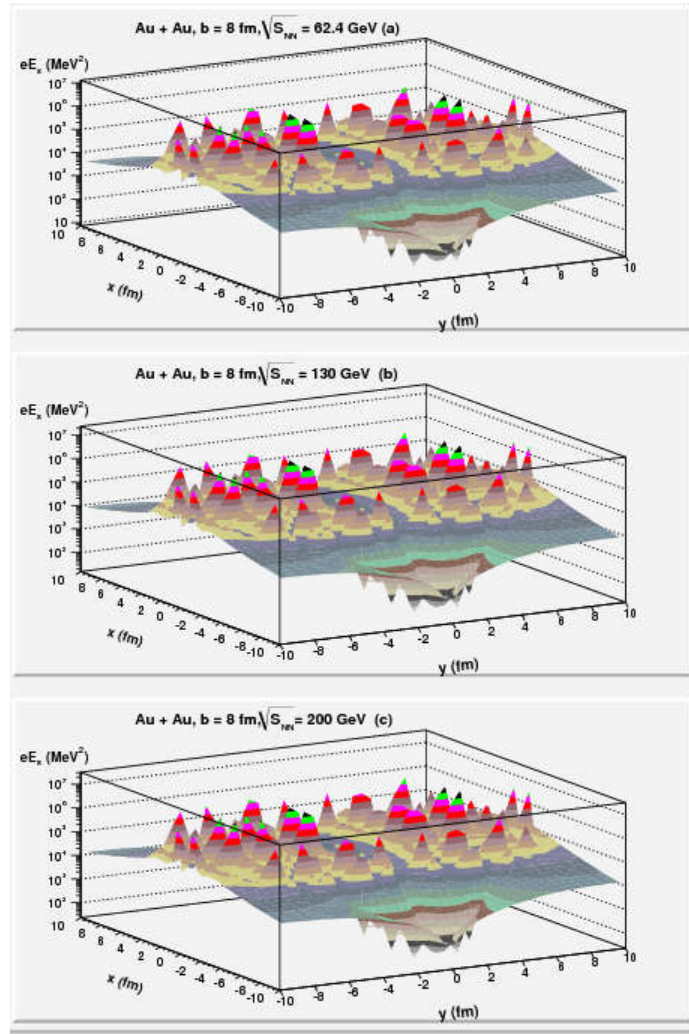


Fig. 1. The dependencies of electric field spatial distributions Of eE_x on different collision energies $\sqrt{s_{NN}} = 62.4$ GeV(a), 130 GeV(b) and 200 GeV(c), respectively. The impact parameters $b = 8$ fm and proper times $\tau = 0.0001$ fm.

Fig.2 shows the dependence of electric field spatial distributions of eE_x on different collision energies $\sqrt{s_{NN}} = 900$ GeV, 2760 GeV and 7000 GeV at proper time $\tau = 0.0001$ fm and impact parameter $b = 8$ fm. The collision energies shown in Fig. 2 are in the LHC energy region. Comparing with Fig.1, we find that with the increasing of collision energy, the eE_x spatial distributions become smoother than that in the RHIC energy region. It is found that when CMS energy $\sqrt{s_{NN}}$ approach 7000 GeV , the eE_x spatial distributions peaks almost disappear and the eE_x spatial distributions become smooth.

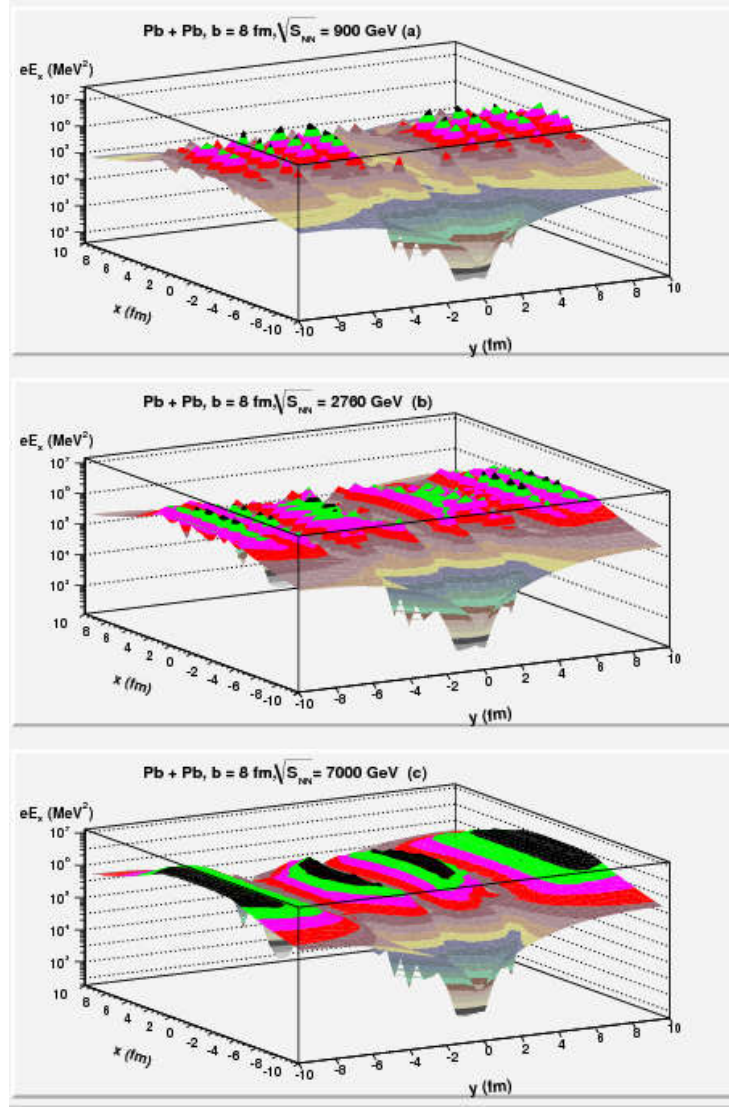


Fig. 2. The dependencies of electric field spatial distributions of eE_x on different collision energies $\sqrt{s_{NN}} = 900$ GeV(a), 2760 GeV(b), 7000 GeV(c), respectively. The impact parameters $b = 8$ fm and proper times $\tau = 0.0001$ fm.

Compared with Fig.1, Fig. 3 shows the dependence of electric field spatial distributions of eE_y at different collision energies $\sqrt{s_{NN}} = 62.4$ GeV, 130 GeV and 200 GeV, at proper time $\tau = 0.0001$ fm and impact parameter $b = 8$ fm. The eE_y spatial distributions are also not smooth distributions, which is same as that of eE_x spatial distributions in the RHIC energy region.

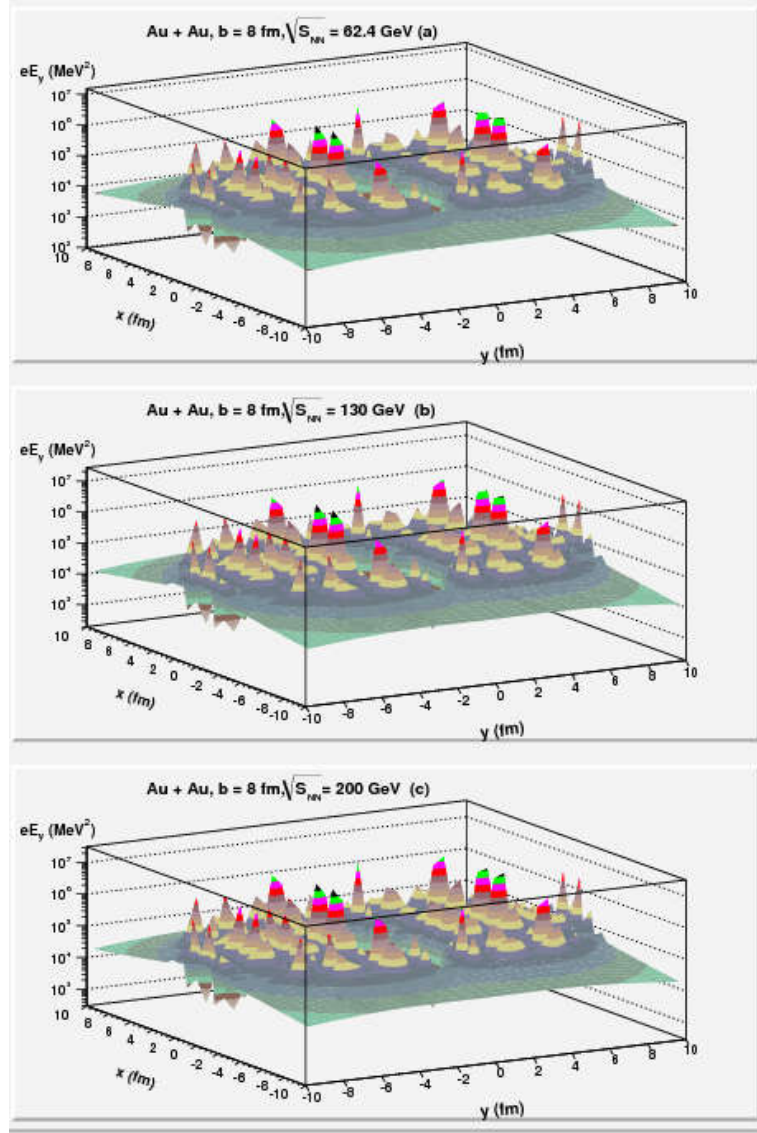


Fig. 3. The dependencies of electric field spatial distributions of eE_y on different collision energies $\sqrt{s_{NN}} = 62.4\text{ GeV}$ (a), 130 GeV (b) and 200 GeV (c), respectively. The impact parameter $b = 8\text{ fm}$ and proper times $\tau = 0.0001\text{ fm}$.

Fig.4 shows the dependence of electric field spatial distributions of eE_y at different collision energies $\sqrt{s_{NN}} = 900\text{ GeV}$, 2760 GeV and 7000 GeV , at proper time $\tau = 0.0001\text{ fm}$ and impact parameter $b = 8\text{ fm}$. The collision energies shown in Fig. 4 are in the LHC energy region. Comparing with Fig.3, one finds that with the increasing of collision energy, the eE_y spatial distributions become smoother than that in the RHIC energy region. One finds that the eE_y spatial distributions at LHC $\sqrt{s_{NN}} = 7000\text{ GeV}$ is a smooth distribution and the distribution peaks

almost disappear. The feature eE_y spatial distribution at LHC is similar to that of eE_x spatial distributions.

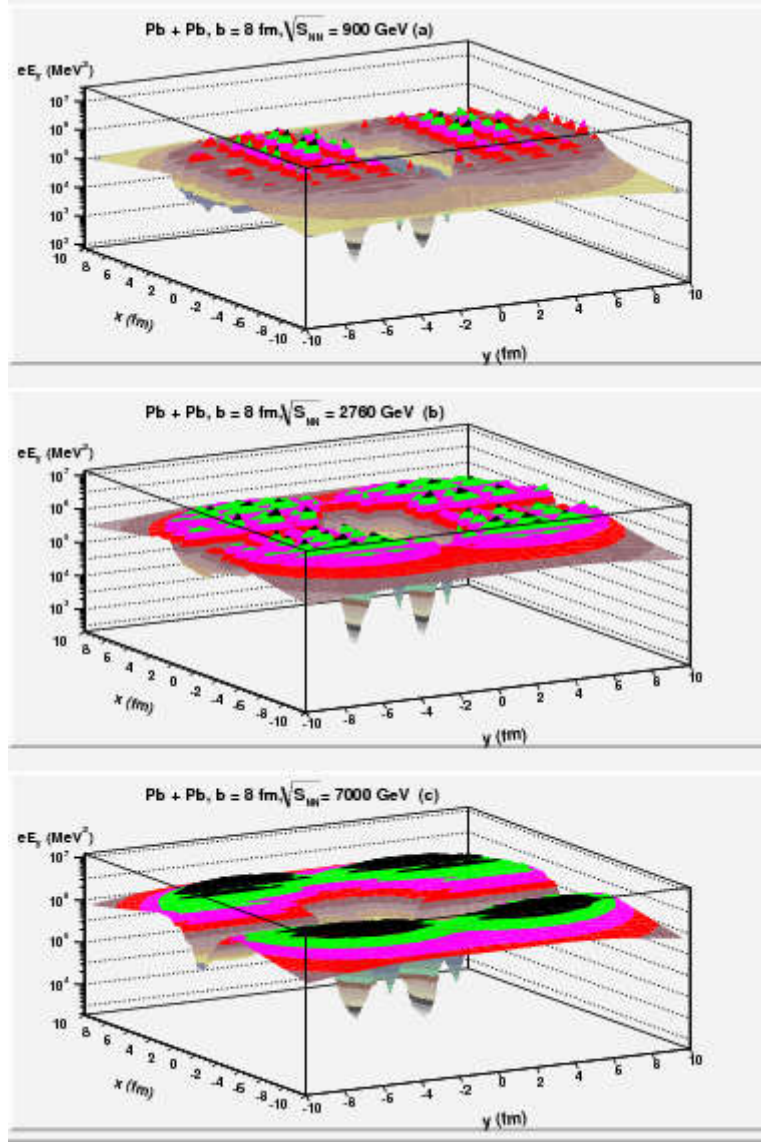


Fig. 4. The dependencies of electric field spatial distributions

of eE_y on different collision energies $\sqrt{s_{NN}} = 900$

GeV(a), 2760 GeV(b) and 7000 GeV(c), respectively. The impact parameter $b = 8$ fm and proper times $\tau = 0.0001$ fm.

3 The electric field of total charges by the produced thermal quarks

At first, let us discuss the evolution of the time and space evolution of the produced thermal quark momentum. According to the theory of the longitudinal collective flow of the relativistic heavy ion collisions, the rapid distribution of the thermal quark is [14-21]:

$$f(Y) = K \int_{-Y_{f0}}^{Y_{f0}} (1 + 2\Gamma + 2\Gamma^2) e^{-1/\Gamma} dY_f \quad (13)$$

where K is the normalized constant, the corresponding function Γ is as follow:

$$\Gamma = \frac{T e^{-(\tau - \tau_0)/\tau}}{m \cosh(Y - Y_f)} . \quad (14)$$

Based on the Fermi-Dirac statistics [22, 23], the charge distribution function of the thermal quark is given as follow:

$$\rho_{q\pm}(\vec{x}'_{\perp}) = K_1 \cdot \frac{\rho_{\pm}(\vec{x}'_{\perp})}{1 + \exp\left\{\left(\varepsilon - \mu_q\right)/T\right\}} , \quad (15)$$

where the nucleon distribution function of the nucleus is:

$$\rho_{\pm}(\vec{x}'_{\perp}) = N \cdot \int_{-R}^R dz \frac{n_0}{1 + \exp\left[\frac{\sqrt{\left(\vec{x}'_{\perp} \mp \vec{b}/2\right)^2 + y^2 + z^2} - R}{d}\right]} , \quad (16)$$

$\varepsilon = \sqrt{m^2 + p_T^2} \cosh Y$ is the thermal quark energy, K_1 is the normalized constant, and μ_q is the quark chemical potential. When $\sqrt{s_{NN}} = 62.4$ GeV, $\mu_q = 1/3 \mu_B = 0.02$ GeV, and when $\sqrt{s_{NN}} = 200$ GeV, $\mu_q = 0.01$ GeV. When $\sqrt{s_{NN}} = 900, 2760$ and 7000 GeV, $\mu_q = 0.005, 0.002$ and 0.001 GeV.

The contribution of the thermal quark to the electric field is:

$$\begin{aligned} e\vec{E}_p^{\pm}(\tau, \eta, \vec{x}_{\perp}) = & \pm ZK\alpha_{EM} \int d^2\vec{x}'_{\perp} \int dY \int_{-Y_f}^{Y_f} dY_f f(Y) (1 + 2\Gamma + 2\Gamma^2) e^{-1/\Gamma} \\ & \times \sinh(Y \mp \eta) \rho_{q\pm}(\vec{x}'_{\perp}) \frac{(\vec{x}'_{\perp} - \vec{x}_{\perp})}{\left[(\vec{x}'_{\perp} - \vec{x}_{\perp})^2 + \tau^2 \sinh^2(Y_0 \mp \eta)\right]^{3/2}} \end{aligned} \quad (17)$$

where proper time is $\tau = \sqrt{t^2 - z^2}$, and pseudo-rapidity is $\eta = \frac{1}{2} \log\left[(t+z)/(t-z)\right]$.

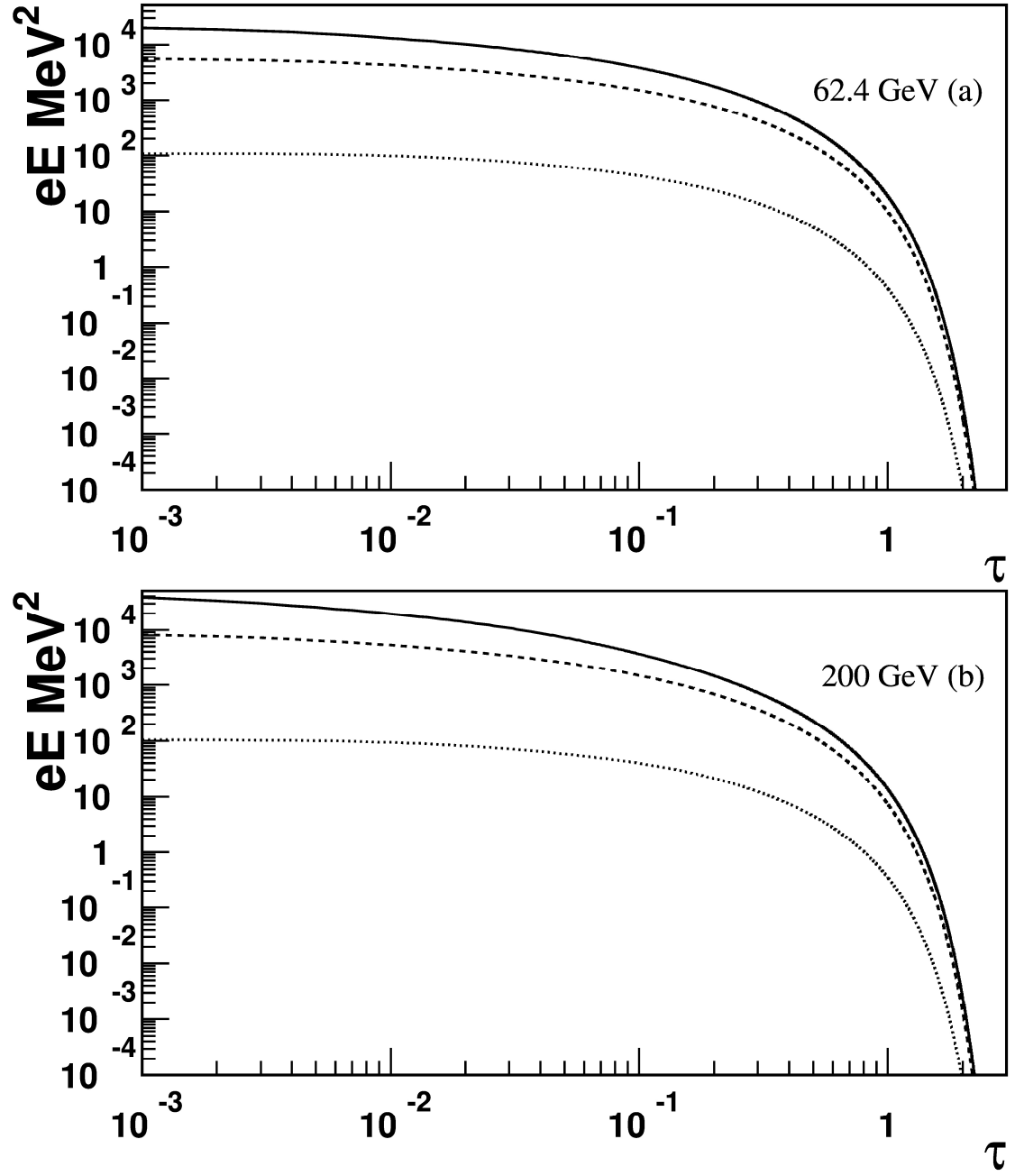


Fig. 5 The dependence of the electric field eE produced by the thermal quark in the central region with different impact parameters on the proper time τ with $\sqrt{s_{NN}} = 62.4$ GeV and 200 GeV in the RHIC energy region. The real line is for $b = 8$ fm, the dashed line is for $b = 8$ fm and the dotted line is for $b = 12$ fm.

Fig. 5 show the dependence of the electric field eE produced by the thermal quark in the central region with different impact parameters on the proper time τ with $\sqrt{s_{NN}} = 62.4$ GeV and 200 GeV in the RHIC energy region. From Fig. 5 (a), one can find that when τ and impact parameter b become smaller and smaller, the electric field eE becomes more and more strong. The maximum of the electric field eE at $\sqrt{s_{NN}} = 62.4$ GeV can reach 4.0×10^4 MeV². As for the periphery collisions, the contribution of produced particles to the electric field eE comes

very small. The electric field formed at the beginning of the collision is only 100 MeV^2 in case $b = 12 \text{ fm}$. At the same time, we find that the electric field decays rapidly with the time evolution, even in the case of $b = 4 \text{ fm}$ collision, the electric field is quickly reduced to about 10^{-4} . Fig. 5 (b) shows the same as that of Fig. 5(a) but for $\sqrt{s} = 200 \text{ GeV}$. It is found that almost the same variation of the electric field with the time τ as the Fig. 5 (a).

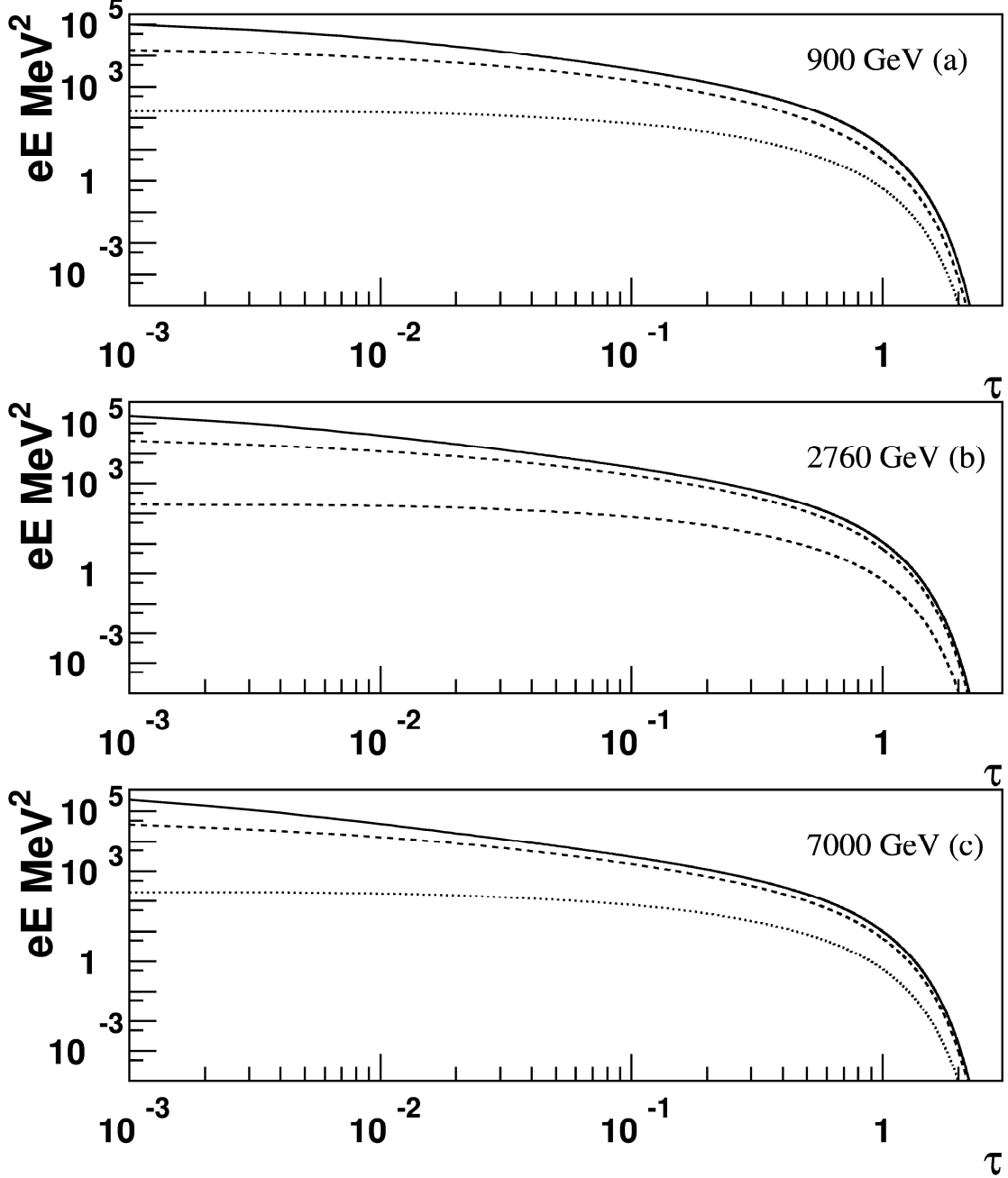


Fig. 6 The dependence of the electric field eE produced by the thermal quark in the central region with different impact parameters on the proper time τ with $\sqrt{s_{NN}} = 900 \text{ GeV}$, 2760 GeV and 7000 GeV in the LHC energy region. The real line is for $b = 8 \text{ fm}$, the dashed line is for $b = 8 \text{ fm}$ and the dotted line is for $b = 12 \text{ fm}$.

Fig. 6 show the dependence of the electric field eE produced by the thermal quark in the

central region with different impact parameters on the proper time τ with $\sqrt{s_{NN}} = 900$ GeV, 2760 GeV and 7000 GeV in the LHC energy region. From Fig. 6, one can find that when τ and impact parameter b become smaller and smaller, the electric field eE becomes more and more strong. The maximum of the electric field eE at $\sqrt{s_{NN}} = 900$ GeV can reach 2.0×10^5 MeV². This value is much larger than that of $4.0 \times 10^4 = 62.4$ GeV in the RHIC energy region.

It is found that the electric field decays rapidly with the time evolution, even in the case of $b = 4$ fm collision, the electric field is quickly reduced to about 10^{-3} . Fig. 6 (b, c) shows the same as that of Fig. 6(a) but for $\sqrt{s_{NN}} = 2760$ GeV and 7000 GeV. It is found that almost the same variation of the electric field with the time τ as the Fig.6(a).

4 Summaries and conclusions

It is shown that an enormous electric field can indeed be created in off-central heavy-ion collisions. The electric field distributions of eE_y and eE_x are highly inhomogeneous which are same as that of magnetic field distributions. The enormous electric field is produced just after the collision, and the magnitude of electric field of LHC energy region is larger than that of RHIC energy region at small proper time. The electric field in the LHC energy region decreases more quickly with the increase of the proper time than that of RHIC energy region. As the proper time τ increases to a certain value $\tau < 8.0 \times 10^{-3}$ fm/c, the magnitude of electric field in the RHIC energy region begins to be larger than that of LHC energy region. These highly inhomogeneous distribution features of electric field in RHIC and LHC energy regions given by this paper will help us to study the experimental results given by RHIC and LHC.

The dependences of electric field spatial distributions of eE_x and eE_y on different collision energies $\sqrt{s_{NN}} = 900$ GeV, 2760 GeV and 7000 GeV at LHC energy region and at $\sqrt{s_{NN}} = 62.4$ GeV, 130 GeV and 200 GeV at RHIC energy region proper time $\tau = 0.0001$ fm and impact parameter $b = 8$ fm are studied in this paper. The collision energies mentioned in this paper covered the whole RHIC and LHC energy regions. It is found that with the increasing of

collision energy, the eE_y and eE_x spatial distributions are more smooth in the LHC energy region than that in the RHIC energy region.

We also study the dependence of the electric field eE produced by the thermal quark in the central region with different impact parameters on the proper time τ in the RHIC and LHC energy region. One can find that when τ and impact parameter b become smaller and smaller, the electric field eE becomes more and more strong. The maximum of the electric field eE at $\sqrt{s_{NN}} = 900$ GeV can reach $2.0 \times 10^5 \text{ MeV}^2$. This value is much larger than that of $\sqrt{s} = 62.4$ GeV in the RHIC energy region. As for the periphery collisions, the contribution of produced particles to the electric field eE becomes very small.

References

- [1] Ma G L, and Huang X G. Phys. Rev. C, 2015, **91**: 054901
- [2] Błoczyński J, Huang X G, Zhang X, and Liao J. Phys. Lett. B, 2013, **718**: 1529
- [3] Skokov V, Illarionov A Y, and Toneev V. Int. J. Mod. Phys. A, 2009, **24**: 5925
- [4] Bzdak A and V Skokov. Phys. Lett. B, 2012, **710**: 171
- [5] Deng W T, and Huang X G. Phys. Rev. C, 2012, **85**: 044907
- [6] Voronyuk V, Toneev V D, Cassing W, Bratkovskaya E L, Konchakovski V P, and Voloshin S A. Phys. Rev. C, 2011, **83**: 054911
- [7] Huang X G, and Liao J. Phys. Rev. Lett. 2013, **110**:232302
- [8] Jiang Y, Huang X G, and Liao J. Phys. Rev. D, 2015, **91**: 045001
- [9] Pu S, Wu S Y, and Yang D L. Phys. Rev. D, 2014, **89**: 085024
- [10] Kharzeev D E, McLerran L D, Warringa H J. Nucl. Phys. A, 2008, **803**:227
- [11] Tuchin K. Advances in High Energy Physics, 2013, **2013**:490495
- [12] Mo Y J, Feng S Q, and Shi Y F. Phys. Rev. C, 2013, **88**: 024901
- [13] Zhong Y, Yang C B, Cai X, and Feng S Q. Advances in High Energy Physics, 2014, **2014**:193039
- [14] Feng S Q, Feng L, and Liu L S. Phys. Rev. C, 2000, **63**: 014901
- [15] Feng S Q and Zhong Y. Phys. Rev. C, 2011, **83**: 034908
- [16] Feng S Q and Xiong W. Phys. Rev. C, 2008, **77**: 044906

- [17] Schnedermann E, Sollfrank J, Heinz U. Phys. Rev. C, 1993, **48**:2462
- [18] Schnedermann E, Sollfrank J, Heinz U. Prog. Part. Nucl. Phys. 1993, **30**: 401
- [19] Cai X, Feng S Q, Li Y D, Yang C B, and Zhou D C. Phys. Rev. C, 1995, **51**: 3336
- [20] Braun-Munzinger P, Stachel J, Wessels J P, and Xu N. Phys. Lett. B, 1995, **344**: 43
- [21] Braun-Munzinger P, Heppel I, and Stachel J. Phys. Lett. B, 1999, **465**:15
- [22] Becattini F, Cleymans J, Keranen A, Suhonen E, and Redlich K. Phys. Rev. C, 2001, **64**: 024901
- [23] Cleymans J and Redlich K, Phys. Rev. Lett. 1998, **81**: 5284